2003-01-1040

Time resolved spray characterisation in a common rail direct-injection production type Diesel engine using combined Mie/LIF laser diagnostics

Marc Uhl
Robert Bosch GmbH

Robert Schießl, Ulrich Maas
Institut für Technische Verbrennung, Universität Stuttgart

Andreas Dreizler
Technische Universität Darmstadt, FG Energie- und Kraftwerkstechnik

ABSTRACT

This study reports on laser-based diagnostics to temporally track the evolution of liquid and gaseous fuel in the cylinder of a direct injection production type Diesel engine. A two-dimensional Mie scattering technique is used to record the liquid phase and planar laser-induced fluorescence of Diesel is used to track both liquid and vaporised fuel. LIF–Signal is visible in liquid and gas phase, Mie scattering occurs only in zones where fuel droplets are present. Distinction between liquid and gaseous phase becomes therefore possible by comparing LIF– and Mie–Signals. Although the information is qualitative in nature, trends of spray evolution are accessible. Within this study a parametric variation of injection pressure, in-cylinder conditions such as gas temperature and pressure as well as piston geometry are discussed. Observations are used to identify the most sensitive parameters and to qualitatively describe the temporal evolution of the spray for real engine conditions.

INTRODUCTION

In-cylinder diagnostics is of growing importance to understand the interaction between fluid mechanics, spray evolution, evaporation and mixing in high-speed, direct-injection Diesel engines. This interaction depends on a variety of parameters such as spray momentum, in-cylinder turbulence, or spray-wall interaction. Due to the complexity of the process, a comprehensive description using computational fluid dynamics is not possible. Therefore, an experimental method is essential that allows to temporally track spray penetration and evaporation even under the harsh conditions of a Diesel engine. This information is important for a more detailed understanding the interplay between large-scale flow-field structures such as swirl and tumble, fine structure turbulence, spray dynamics, and spray-wall interaction.

Different optical techniques have been discussed that are feasible for a phase discrimination, such as exciplex laser-induced fluorescence [i,ii,iii,iv,v,vi,vii] (LIF) or simultaneous Mie scattering in combination with fuel LIF [viii,ix]. Exciplex–LIF relies on a composition of tracers added to a non-fluorescing model fuel, that exhibits shifted emission bands of its liquid relative to its gaseous phase. Using proper calibration, in general, the exciplex LIF method is capable to quantitatively determine evaporation. A blend of single components allows to generate a fuel with evaporation properties comparable to real fuel [x,xi]. This technique has been used successfully to investigate in-cylinder Otto engine performance but is restricted to idealised conditions. Applied on realistic direct-injection Diesel engines, however, the exciplex technique suffers from the need to replace real Diesel by a model fuel. In addition, presence of oxygen complicates the quantification of the evaporation process due to fluorescence quenching and thereby the most promising potential of the technique is lost. Technical difficulties arise from the fact that exciplex LIF needs a fuel/tracer mixture free of contamination. These conditions are difficult to achieve in a common rail system. Moreover, lubrication of the injector by model fuel is poor and results in relatively short service life.

In contrast, the measurement of Mie–scattering and fuel–LIF is comparatively easily applicable to realistic Diesel engines. It therefore offers the higher potential to track the temporal evolution of spray penetration and evaporation in a production type Diesel engine. The technique is based on Mie scattering from fuel droplets

and LIF from fuel, both in gaseous and liquid phase. A phase discrimination becomes possible by subtraction of LIF and Mie signals. It has to be noticed that this technique is qualitative in nature. High signal levels enables its application even for fouled optical access.

The application of the combined Mie/fuel LIF technique to a production type direct-injection common rail Diesel engine is discussed. To investigate the influence of spray momentum, the rail pressure has been varied from 500 to 1800 bar. To examine the role of in-cylinder gas pressure and temperature, these quantities have been varied by using different intake pressures and temperatures. The studies have been carried out for a disc shaped and Ω-shaped combustion chamber, respectively. For the first case, a flat piston crown was used, for the latter a bowl typical for this kind of engines was used.

EXPERIMENTAL SET-UP

OPTICALLY ACCESSIBLE ENGINE

The engine was based on a single-cylinder crank shaft case (Hatz) mounted to a production type four valve cylinder head. To allow for laser based spray diagnostics the upper part of the cylinder wall was replaced by a quartz ring. By these means laser sheets could access the top part of the combustion chamber from all directions. Laser-induced signals were monitored perpendicularly to the laser beams. For this purpose the piston was equipped with a fused silica crown, either flat or with an Ω-shaped piston bowl typical for direct injection Diesel engines. The lower surface of the piston crown was curved to collimate signal radiation. The piston was lengthened and slitted similar to the design first presented in [xii] to image the measurement volume onto the 2D array detectors by using a fixed mirror inside the piston. A cross section of the engine is shown in figure 1. The most important engine parameters are listed in table 1. The engine could be motored up to 3,000 rpm but the operating point in this study was fixed to 1,500 rpm. This set-up allowed us to fill the engine with pure nitrogen instead of air. Pressure transducers (Kistler) were used to record temporally resolved pressure traces for every cycle. Thermocouples in the intake duct, the exhaust pipe system and the cylinder head were used to control stationary operation of the engine. The intake gas could be charged up to 2 bar and heated up to 375 K. The gas flow in inlet and exhaust pipes was modelled using a simple one-dimensional code (AVL BOOST), enabling us to predict the volumetric efficiency. By this means thermodynamic properties were calculated and checked for close similarity to modern production type Diesel engines.

The injector used was a production type six orifice device, each hole 152 µm in diameter and 1.05 mm long. A sensor monitored the correct stroke of the needle. In the common rail, the fuel pressure could be varied from 500 to 1,800 bar. During one cycle up to three injections were feasible although in this study only two injections per cycle were utilised. Regular, desulphurized Diesel fuel (DEA) was used throughout the study. Table 2 summarises the most important operation parameters of the engine.

OPTICAL LAYOUT OF SPRAY DIAGNOSTICS

The diagnostics were aimed to temporally resolve penetration of the liquid as well as evaporated fuel into the combustion chamber. Therefore a combination of two-dimensional laser Mie scattering and planar laser-induced fluorescence (PLIF) has been chosen. Mie scattering is capable to visualise spray droplets while PLIF - following resonant excitation of Diesel fuel - can be used to track both the liquid and the gas phase. Using the current set-up the dynamic range of the Mie technique was estimated to be capable to record droplets in a range from 2 to 30 µm. Under the assumption that no second wind induced breakup of droplets occurs and that D^2-law for droplet evaporation is applicable, we can estimate that the dynamic range of the Mie-technique is capable to record droplet sizes in a range from 2 µm to 30 µm [xiii].

By comparing the two-dimensional appearance of the Mie and PLIF signals a discrimination between liquid and gaseous phase of the fuel becomes possible. Notice that this procedure accounts droplets smaller than 2 µm as “evaporated”. This introduces a systematic error not accounted for in the subsequent discussion. Therefore, the data presented is only qualitative in nature and gives relative trends for the parametric variation to be shown.

For Mie scattering a Q-switched frequency doubled Nd:YAG laser operating at a wavelength of 532 nm and 20 kHz pulse repetition rate (Spectra Physics) was employed. Using this wavelength, absorption of the laser beam was not significant and no additional fluorescence signals were produced by the Nd:YAG laser. For fuel PLIF a broadband XeCl excimer laser was employed. Due to the lower repetition rate of this laser only one PLIF image per cycle was recorded. The radiation around 308 nm efficiently excited fluorescence of liquid as well as gaseous fuel. As shown in figure 2, the radiation of both lasers was split into two separate beams of equal intensity that entered the combustion chamber from opposite directions. In this way spatial intensity variations due to extinction could be minimised. All laser beams were formed to sheets 40 mm wide and 1 mm thick. Additionally, indirect laser light was present that was reflected from the glass walls or scattered from liquid spray components. This indirect laser light made a significant contribution to the illumination of the combustion chamber, reaching regions that were not accessed directly by the laser sheet. This resulted in a fully illuminated combustion chamber, Mie and PLIF signals were collimated by the lower, curved surface of

the piston crown and directed to the detection unit. A dichroic mirror separated Mie scattering at 532 nm from broadband fuel fluorescence between 350 and 430 nm. Mie scattering was detected temporally resolved using an eight-channel intensified CCD detector device (IMACON 468, Hadland Photonics). In this way a temporally resolved sequence of up to eight Mie images was monitored at typically $2x10^4$ Hz. This high temporal resolution allowed for monitoring real-time spray development during one cycle. One PLIF image was synchronised relative to one of these Mie exposures using a single frame intensified CCD camera (PCO). Figure 3 demonstrates the information gathered by using this set-up.

DATA REDUCTION

Before data post-processing every image was corrected for distortions along the signal path caused by the curved piston window. The distortion field was measured on some control points defined by a regular grid template placed on the piston. Then, the distortion for every image pixel was calculated by local bicubic interpolation of the control points. Mie and PLIF data were analysed for radial as well as tangential penetration depth, penetration velocity and projected area.

RESULTS AND DISCUSSION

PENETRATION OF LIQUID FUEL

In a first step the penetration of liquid fuel into the chamber is analysed using temporally resolved Mie scattering only. Employing a flat piston crown, the spreading of the spray is undisturbed by interactions with the wall while spray-wall interaction heavily influences the spray development in case of the Ω-shaped piston crown. The employed imaging technique projects a three-dimensional scene onto a two-dimensional plane; our measurement therefore delivers only the radial component of the penetration. The "real" penetration measured along the central spray plum axis and the measured radial penetration do not differ significantly, as the tilt angle of the spray central axis versus a horizontal line is only 10 degrees.

Flat piston crown

Using the flat piston crown the spray penetration is limited by the cylinder diameter. The distance between the centrally mounted injector and the cylinder wall is 39 mm. For all investigations shown the motored engine speed, the cylinder head temperature, and the cylinder temperature are fixed to 1,500 rpm, 80°C, and 140°C, respectively (compare table 2). The injected volume was kept constant at the same value of 1,5 mm^3 (Pilot Injection) and 30 mm^3 (Main Injection) for each injection pressure. This was calibrated by EMI (Injection Mass Indicator). In the intake duct pure nitrogen has been used to allow observation of spray development, evaporation, and mixing undisturbed by the strong light emission of soot that is typical for fired Diesel-cycles.

Figure 4 shows an exemplary spray development as a sequence of 29 Mie images. In this case the injection pressure is 800 bar and nitrogen pressure and temperature in the intake duct are 1,600 mbar and 25°C, respectively. Time intervals between successive images are 50 µs. Times are relative to the injector triggering signal (Start of Energizing, SOE). Notice, that only up to eight Mie images could be recorded during one cycle. Therefore the sequence in figure 4 is composed of four individual cycles with temporally shifted exposures. It is obvious that the spray cone of each of the six orifices is approximately symmetric. Only small differences between the single spray cones are observed. The first appearance of the spray is recorded 400 µs after the injector trigger. This delay can be explained by the dynamics of the injector and more specifically by the material dynamics of the needle. Subsequently, the spray penetrates into the combustion chamber until it reaches a maximum penetration depth at around 800 µs. The spray pattern is approximately constant for times between 800 and 1,600 µs where the injector is closed. At 1,800 µs the spray completely vanished. Notice, that the disappearance of the spray ensues synchronously over the entire spray. This indicates that droplets sprayed from the injector during the needle closure have very low velocity and therefore evaporation takes place close to the nozzle exit.

Using data as presented in figure 4 the penetration of the spray can be determined temporally resolved. In figure 5 the temporal evolution of the spray penetration is compared for four different injection pressures and two different pressures in the intake duct. Note that the analysis is for the radial component of the penetration. For times up to 800 µs a strong variation of the spray evolution is observed for varying injection pressures. Increasing injection pressures results in a faster spray expansion. The maximum penetration depth, however, is not dependent on the injection pressure for a fixed engine load. Decreasing the cylinder pressure at TDC by 25 % (1,200 mbar instead of 1,600 mbar in the intake duct) is followed by a slight increase of penetration depth of approximately 10%.

The spray evolution can be subdivided into three regimes. In a first period the spray penetrates into the chamber with an almost constant velocity. This is indicated by the nearly linear dependence of the spray penetration on process time. The second regime is characterised by the deceleration of the spray expansion. Independent of the injection pressure starting from a penetration depth of 15 mm, the spray is decelerated due to frictional forces until the spray expansion is stopped completely. The third regime is characterised by a temporally constant spray extension. This indicates a dynamic equilibrium between supply of

liquid fuel and its evaporation. With increasing injection pressure the duration of the first and second regime is decreasing. By changing the injection pressure from 500 to 1,800 bar, attainment of the maximum penetration is halved to approximately 400 µs. Variation of the engine load by decreasing the intake duct pressure from 1,600 to 1,200 mbar is of no significant influence on the first period. The deceleration by frictional forces in the second regime, however, is less pronounced for decreased engine load and the maximum penetration depth in the third regime is enhanced.

The influence of the intake duct temperature is shown in figure 6a. In general, the increase of the intake duct temperature only slightly increases the cylinder pressure at TDC. Using a simplified thermodynamic one-dimensional description of the engine (AVL-code BOOST) an increase of the intake duct temperature from 25°C to 100°C results in a decrease of the cylinder pressure at TDC from 57 to 52 bar. The cylinder gas temperature, however, increases from 830 to 880 K. As to be seen from figure 6a the first and second period of the spray evolution is not significantly influenced by an increased temperature. In contrast, the maximum penetration depth is reduced by 15%. This hints to an enhanced fuel evaporation. Using a constant nitrogen gas density in the intake as shown in figure 6b, the spray evolution differs for all three regimes. The enhanced frictional forces lead to a slower spray penetration for the higher cylinder pressure while the higher gas temperature speeds up fuel evaporation [xiv].

Ω-shaped piston

Using the flat combustion chamber presented in the previous section the flow field differs significantly from production type engines. Therefore the piston crown has been changed to a geometry showing the typical Ω-shaped bowl. The geometry of the Ω-shaped bowl is nearly identical to a geometry currently used in a production type engine. The Ω-shaped bowl introduces additional swirl and tumble to the engine load [xv] and therefore strongly affects fuel-air mixing. In addition, the spray impinges on the walls of the bowl and thereby changes the spray appearance dramatically.

Analogous to the investigation using a flat piston crown the injection pressure as well as intake duct pressure and temperature have been varied. Figure 7 exemplary shows a temporal sequence of Mie images for an injection pressure, intake gas pressure and temperature of 800 bar, 1,600 mbar, and 25°C, respectively. For all times the liquid phase is observed to be restricted to the interior of the Ω-shaped bowl. After approximately 650 µs the spray impinges on the wall and spreads out clock- as well as anti-clock wise along the curved walls. Notice, that the swirl direction is anti-clock wise. From detailed investigations of spray-wall interaction [xvi,xvii] it is well known that in the vicinity of locations where the spray impacts on the wall eddies are formed. The structure of these eddies, however, is not spatially resolved in the current study because the focus is on the general spray evolution. After 800 µs differences in the single spray patterns from shot to shot are relatively small. Starting from 1,400 µs the spray patterns start to vanish, in the first place close to the injector.

Data as presented in figure 7 are corrected for optical distortion introduced by the Ω-shaped bowl. Subsequently, the clock- and anti-clock wise spreading of the spray is analysed. Figure 8 shows the penetration depth relative to the location of the spray impact on the wall. The most important observation is that the spray penetration depth in clock-wise direction is only slightly shorter than and in anti-clock wise direction. Note that for the highest in-cylinder pressure of 60 bar investigated in this study the clock- and anti-clock wise penetration are nearly symmetric. This indicates a minor impact of the gaseous turbulent flow field on the trajectories of the liquid phase. One can conclude from this observation that the droplet trajectories are driven by the initial momentum at the injector exit. The maximum tangential penetration depth is –within the uncertainty of the analysis– independent of the injection pressure (not shown) but strongly dependent on the cylinder pressure. Increasing the maximum in-cylinder pressure by 38 % reduces the tangential penetration depth by 2—3 mm. In no case the patterns of neighbouring sprays overlap. Similar to the observations for the flat piston crown, the increase of the cylinder temperature from 830 to 880 K by changing the intake duct temperature results in significant decrease of the tangential penetration depth up to 40%.

PENETRATION OF LIQUID AND GASEOUS FUEL

For the investigation of both the liquid and the gaseous fuel Mie scattering is combined with fuel LIF. Differences between the patterns observed by LIF to those recorded by Mie scattering are attributed mainly to gaseous fuel (bear in mind that Mie scattering was capable to detect minimal droplet diameters of 2 µm only). By these means a distinction of both phases becomes possible that is appropriate for the study of general temporal spray evolution aimed in this study. Analogously to the investigation of the liquid phase using Mie scattering only, the combined Mie/LIF technique has been applied to both the flat as well as the Ω-shaped bowl piston crown.

Flat piston crown

Figure 9 shows the temporal spray evolution as observed by the combined Mie/fuel LIF technique. Notice, that this sequence is not real time from a single cycle but composed from 15 individual cycles due to the low repetition rate for the LIF set-up. For this example

the injection pressure is 800 bar and the intake duct temperature and pressure are 25°C and 1,600 mbar, respectively. Up to 200 µs, the appearance of the spray structures observed by both techniques is quite similar. Subsequently, differences evolve especially at the tips of the spray cones where cloudy structures are formed. It is believed that these structures are due to evaporated fuel. The cloudy structures are extending with time until evaporated fuel from neighbouring spray cones merge. In contrast the liquid phase as observed by Mie scattering does not change its structure significantly until it is completely evaporated. However, homogenisation is not completed for intervals investigated here.

For increased injection pressure the differences between Mie- and LIF-observed spray structures occur at earlier process times (not shown). This could be an indication for reduced droplet diameters at higher injection pressures followed by an enhanced evaporation rate.

Using data from figure 9 the temporal penetration depth is quantified similar to figure 5. Figure 10 compares the evolution of the liquid to the gaseous phase. Differences at the spray tip start up at approximately 400 µs. Spray patterns observed by LIF extend until they reach the cylinder wall and show less deceleration compared to the patterns observed by Mie scattering. In contrast, for all cases liquid fuel observed by Mie scattering reached a constant penetration depth. From this observation one can conclude that evaporated fuel takes over the momentum of the liquid phase and hereby is driven by the initial momentum gained at the injector exit. In addition, evaporated fuel precedes the liquid and spreads over a temporally increasing region. Increasing injection pressures speed up the temporal evolution but do not principally change the process. A more detailed study, of course, should focus on the temporal development of the droplet diameter distribution and is planned for future investigations.

A magnification of single spray cones as shown in figure 11 visualises the influence of the swirl upon the vaporised fuel. In direction of the swirling engine load, the tangential extension is much larger than in the opposing direction. For decreasing injection pressures gaseous fuel drifts are observed for locations closer to the injector. For injection pressures of 1,800 bar gaseous fuel only is observed in front of the liquid spray tip and less influenced by swirl. According to [xviii,xix,xx], for high injection pressures strong gas entrainment is reported. This entrainment prevents evaporated fuel to be spread out at the root of the spray close to the primary break-up region.

For enhanced cylinder pressures the expansion velocity of the liquid spray is retarded (compare figure 5). A corresponding behaviour is observed for the gaseous fuel. Increasing the intake duct temperature from 25°C to 100°C enhances the evaporation rate. This can be seen from figure 12 that compares the areas of observed fuel LIF signals for different process times.

Ω-shaped piston

To investigate the influence of spray–wall interaction and realistic in-cylinder flow fields, similar investigations using the combined Mie/fuel LIF technique have been carried out for the Ω-shaped piston crown. Figure 13 compares LIF sequences for 500 and 1,800 bar, respectively. With increasing injection pressure a more rapid spray evolution is observed. For 500 bar the spray impinges on the wall 1,000 µs after injection trigger while for 1,800 bar this time is reduced to 600 µs. Approaching the end of the fuel injection, striking differences between spray patterns for the different rail pressures are apparent.

The tangential penetration depth of the gaseous fuel is compared to the respective liquid penetration depth in figure 14. Clock- and anti-clock wise penetration differ significantly for gaseous fuel but – as discussed in figure 8 – are nearly symmetric for the liquid fuel. In average the clock and anti-clock wise penetration is 8 and 12 mm, respectively, before the patterns of neighboured gaseous sprays merge. The tangential penetration is clearly asymmetric for the 500 bar case, but nearly symmetric using 1,800 bar. For the highest injection pressure the temporal evolution is more than twice as fast compared to the 500 bar case.

By increasing the in–cylinder temperature from 830 to 880 K the penetration depth of gaseous fuel is not affected but the penetration depth of the liquid fuel decreases (compare previous section). This means that the vaporised fuel volume is increasing with temperature in accordance to an enhanced evaporation rate.

CONCLUSIONS

The aim of this study was to qualitatively investigate the general temporal development of a fuel spray in a modern direct injection Diesel engine. For this purpose an optically accessible single one-cylinder Diesel engine was designed using a production type four-valve cylinder head. The engine performance was close to real conditions. Fuel was injected using a standard common-rail six-orifice nozzle and the range of injection pressures was enlarged compared to conventional common rail systems up to 1,800 bar. A combination of Mie scattering and fuel LIF was used to study the temporal evolution of the liquid and the gaseous fuel. Mie scattering recorded the liquid phase, and LIF both liquid and gaseous phase. Due to the limited dynamic range of the eight-channel ICCD device used for Mie scattering, droplets in a range between 2 and 30 µm were resolved. The phase discrimination relied on subtraction between spray structures observed by Mie scattering and LIF. Hereby droplets smaller than 2 µm were accounted for to be

vaporised. Therefore the data presented are not absolute but give relative trends for the parametric variation.

To study the influence of injection as well as in-cylinder conditions upon the spray evolution the injection pressure and the intake duct pressure and temperature were varied. To more clearly extract the influence of spray-wall interaction in addition to realistic swirl and tumble motion, the study has been conducted for a simple flat and a realistic Ω-shaped piston crown.

In a first step the evolution of the liquid phase of the spray has been investigated solely. An increase of the injection pressure resulted in a speed up of the spray penetration but did not enhance the penetration depth. From this observation it was concluded that the penetration depth of the liquid is determined by the in-cylinder temperature. This was supported by variation of the intake duct temperature from 25 C to 100 C that resulted in a temperature rise from 830 to 880 K according to simplifying thermodynamic engine simulations. A reduction of the in-cylinder pressure was of minor influence and only modified the penetration depth slightly. As expected, spray-wall interaction in connection with realistic gas motion spreads out the liquid phase in tangential direction along the wall of the Ω-shaped bowl.

In a second step spray evolution of both liquid and gaseous phase has been investigated using the above mentioned combined Mie/fuel LIF technique. Ahead of the tip of the liquid phase fuel evaporation is manifested by cloudy structures that show strong dependence on engine load motion. The lower the injection pressure the closer to the injector evaporation starts. This indicates large differences in gas entrainment as already observed by other investigations. It is obvious that an Ω-shaped bowl strongly affects spray evolution compared to a simple flat piston crown. Although these studies have been carried out using inert nitrogen in the intake to prevent combustion it is believed that general trends still are valid for the combusting case. For an improved understanding, however, more quantitative in-situ measurements, such as phase-Doppler anemometry, are necessary to resolve spray droplet distributions.

CONTACT

Marc Uhl, Injection Systems Diesel, Dept. DS/EAC1, Robert Bosch GmbH (e-Mail: marc.uhl@de.bosch.com).

FIGURE CAPTIONS

Engine Type	Single Cylinder
Displacement (cm^3)	410
Stroke (mm)	85
Bore (mm)	78,3
Piston Bowl Volume (cm^3)	16,5
Compression Ratio	18,5
Number of Valves	4
Engine Speed nmax (1/min)	3000
Max. In-Cylinder Pressure (bar)	150
Max. Charge Pressure (mbar)	2000
Injection System	Common Rail

Table 1 Technical data of the 4-valve direct injection Diesel engine.

Engine Speed (1/min)	1500
Temperature of Cylinder Head (°C)	85
Temperature of Piston Liner (°C)	140
Volume of Pre Injection (mm³)	1,5 (at 21° BTDC)
Volume of Main Injection (mm³)	30 (at 2° BTDC)
Turbo Charge Pressure (mbar)	1000, 1200, 1400, 1600
Charge-Air Temperature (°C)	25, 50, 75, 100
Max. In-Cylinder Pressure (bar)	(38-60)
Max. In-Cylinder Temperature (°C)	825-880
Injection Pressure (bar)	500, 800, 1350, 1800
Volume Fraction of Oxygen in Charge Air (%)	0 (Pure Nitrogen) 21 (Air)

Table 2 Operation conditions. In this study pure nitrogen has been used as load to allow for temporally resolved investigation of spray spreading, evaporation, and mixing. Parameters that have been varied are pressure of the injection as well as pressure and temperature of the load (nitrogen). The latter two parameters influence conditions at top dead centre (TDC).

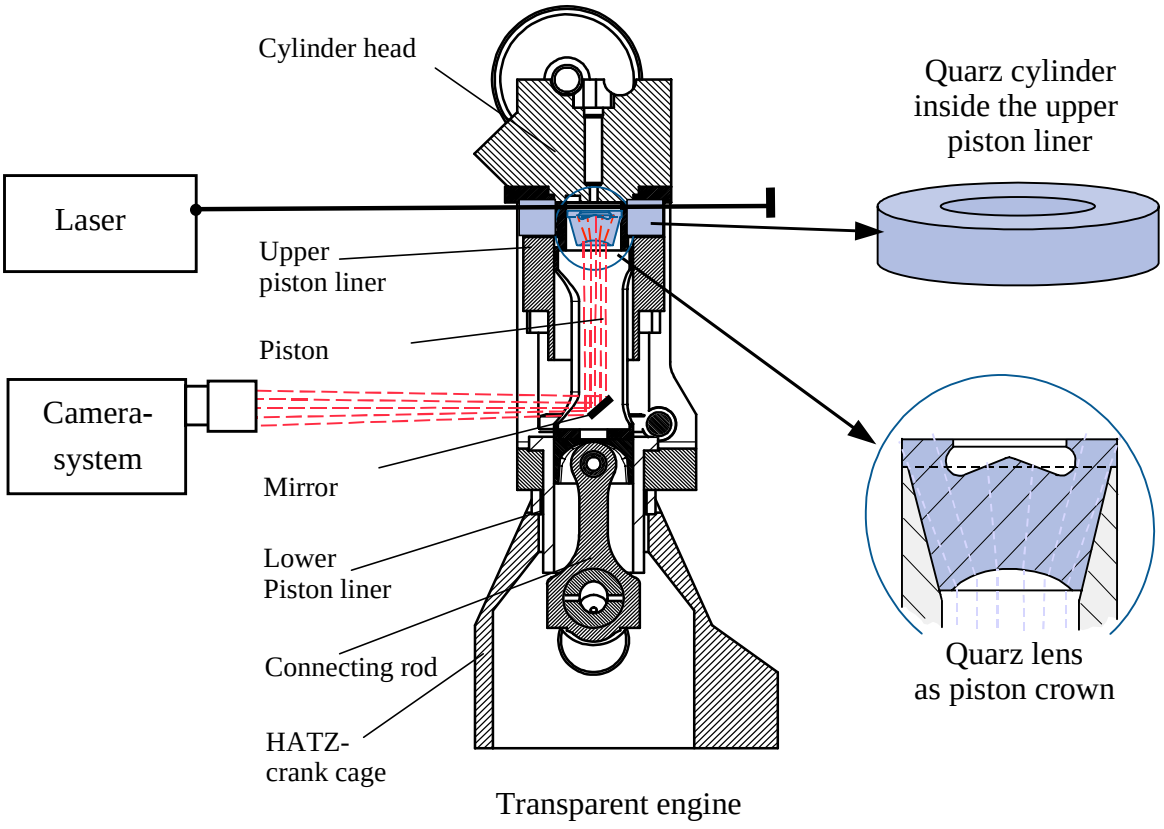

Figure 1 Cross-section of the optically accessible one-cylinder Diesel engine. Laser radiation can enter the combustion chamber through a quartz ring and laser-induced radiation is monitored through the piston crown. The lower side of the piston crown is curved to collect to allow observation of the full combustion chamber.

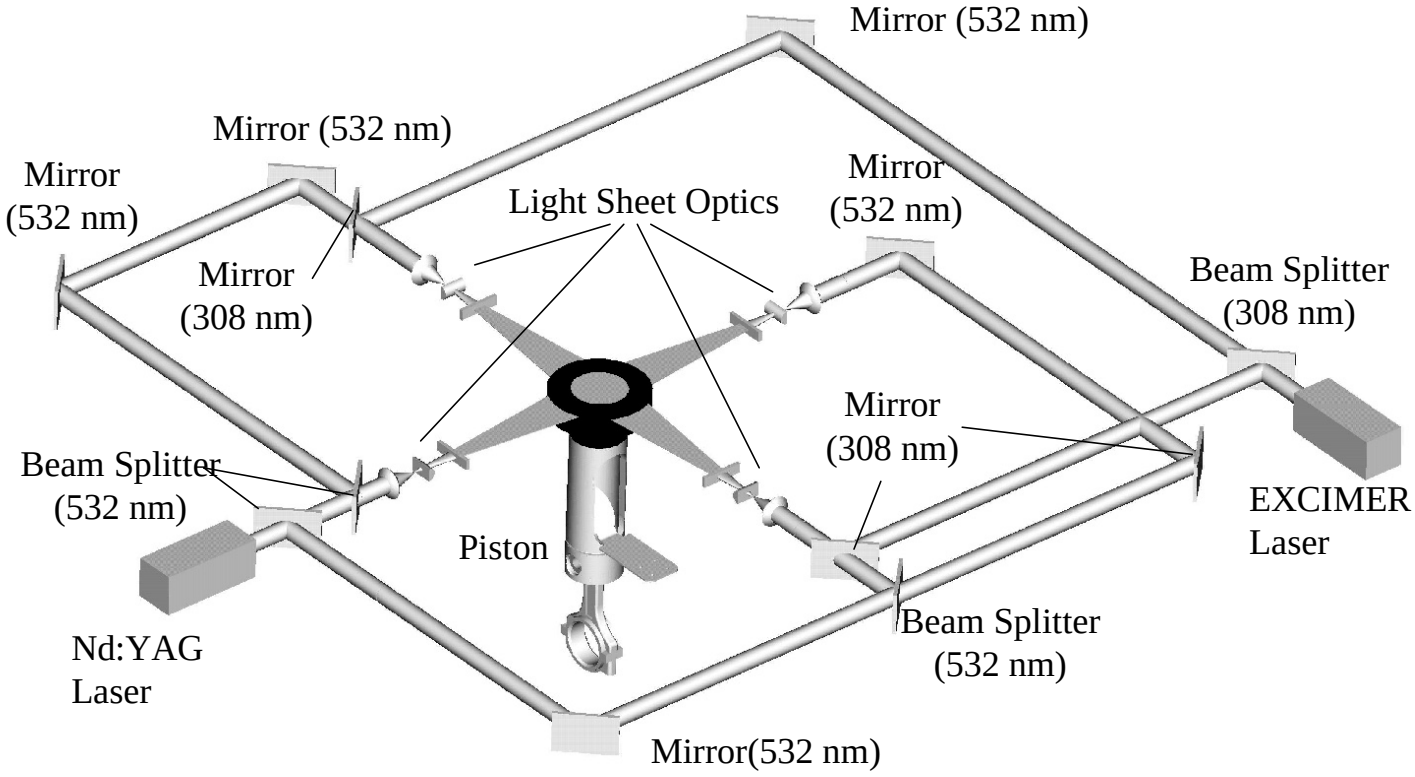

Figure 2 Optical set-up of the combined Mie/LIF technique. The radiation of the Nd:YAG laser is split into four, the radiation of the EXCIMER laser is split into two equally intense beams that enter the combustion chamber from opposite directions. By this means extinction effects are minimised. Mie scattering and LIF are observed by individual ICCD cameras. Notice, that Mie scattering is recorded temporally resolved at typical repetition rates of $2x10^4$ Hz using an eight-channel ICCD device.

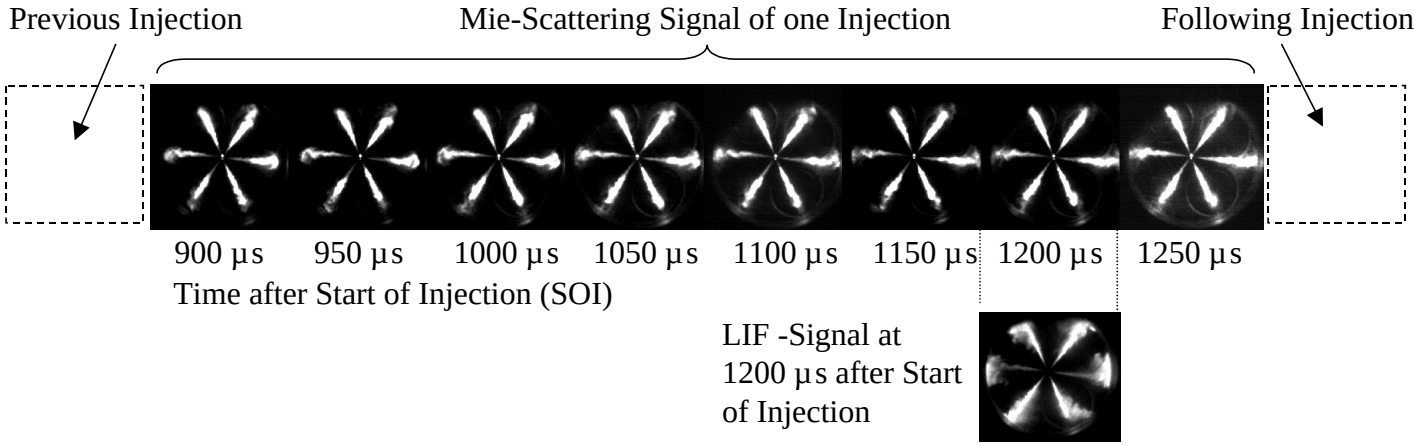

Figure 3 During one cycle eight Mie images and LIF image are recorded. The LIF image is synchronised to one of the Mie images. Higher repetition rates of the LIF detection are prohibitive due to the excimer laser used.

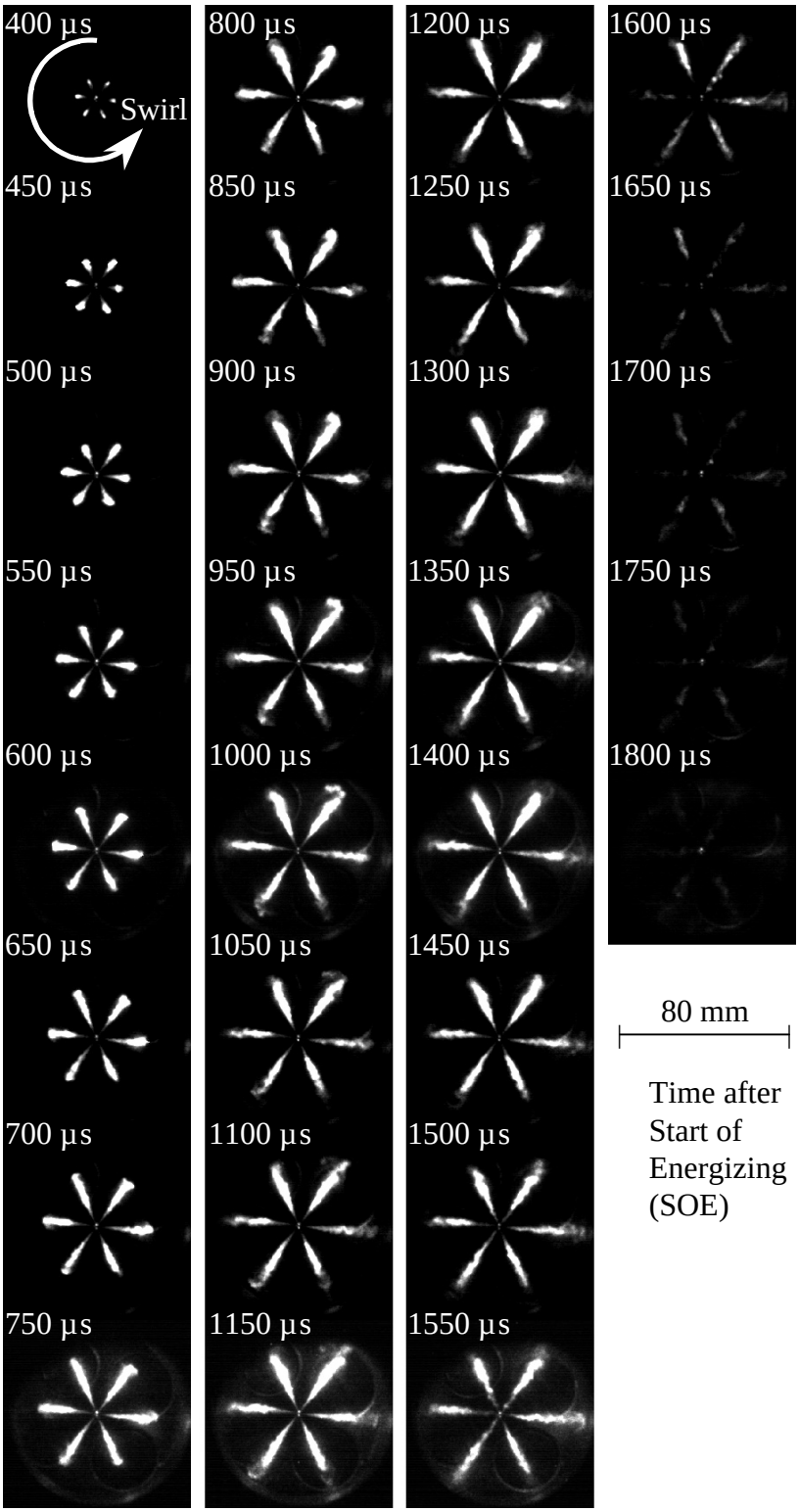

Figure 4 Temporal development of liquid spray in the motored engine. Times inserted in the individual exposures are relative to the trigger signal lifting the needle of the fuel injector. This trigger was fired 2°CA before TDC. For this sequence a injection pressure of 800 bar was used. Pressure and temperature in the intake duct were 1600 mbar and 25°C.

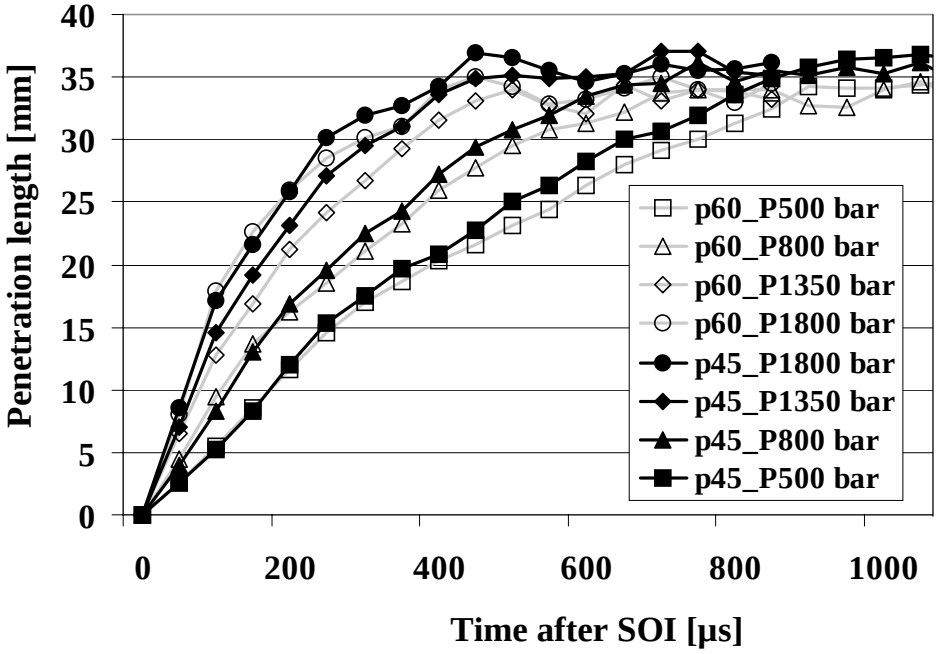

Figure 5 Comparison of the temporal evolution of the spray penetration into the combustion chamber. Time is relative to the first appearance of the spray in the combustion chamber. Each data point shown is an average of all six holes of the injector. The injection pressure is varied between 500 and 1800 bar as indicated in the figure. Nitrogen pressure in the intake is either 1200 (denoted with prefix p45 in the legend, black lines) or 1600 mbar (p60, gray lines). Using a constant intake temperature of 25°C this results in cylinder pressures at TDC of 45 and 60 bar, respectively.

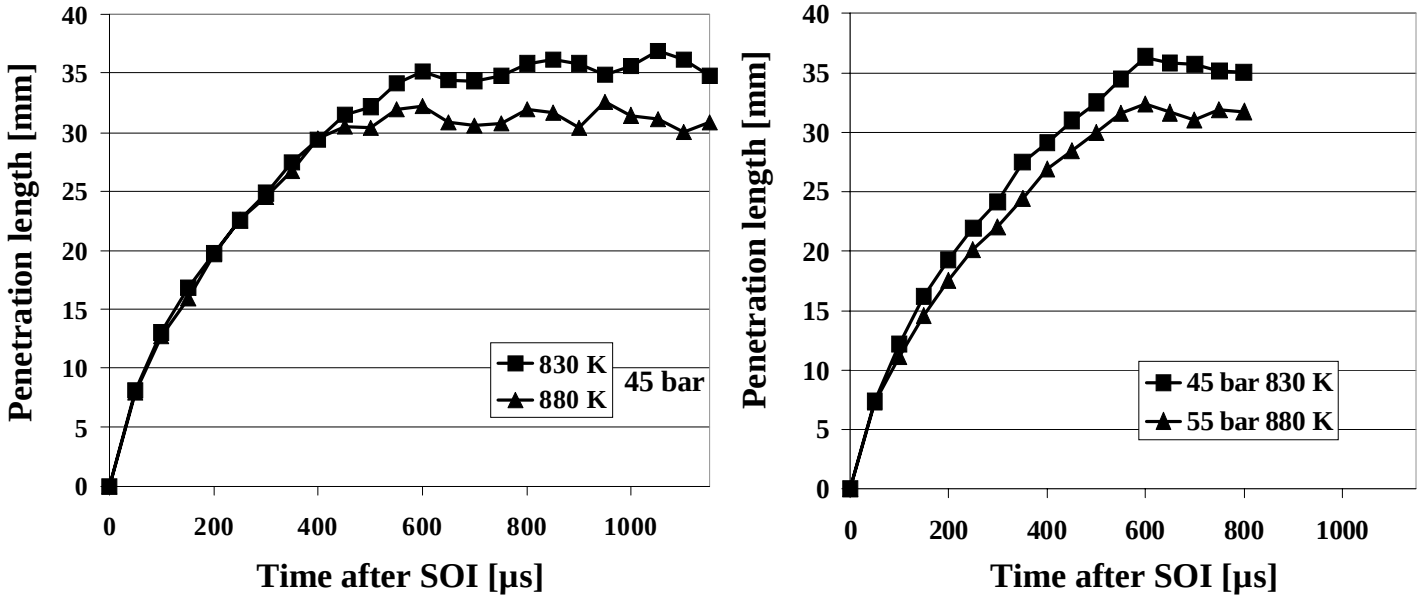

Figure 6 (a): Comparison of a variation of the intake duct temperature. The temperature has been changed from 25°C to 100°C. In both cases the cylinder pressure at TDC is 45 bar and the injection pressure is 800 bar. **(b):** Same temperature conditions as in part (a) but additional variation of intake duct pressure to achieve a constant density of 1.347 kg/m^3 in the intake. Resulting cylinder conditions at TDC are 45 bar, 830 K and 55 bar, 880 K, respectively.

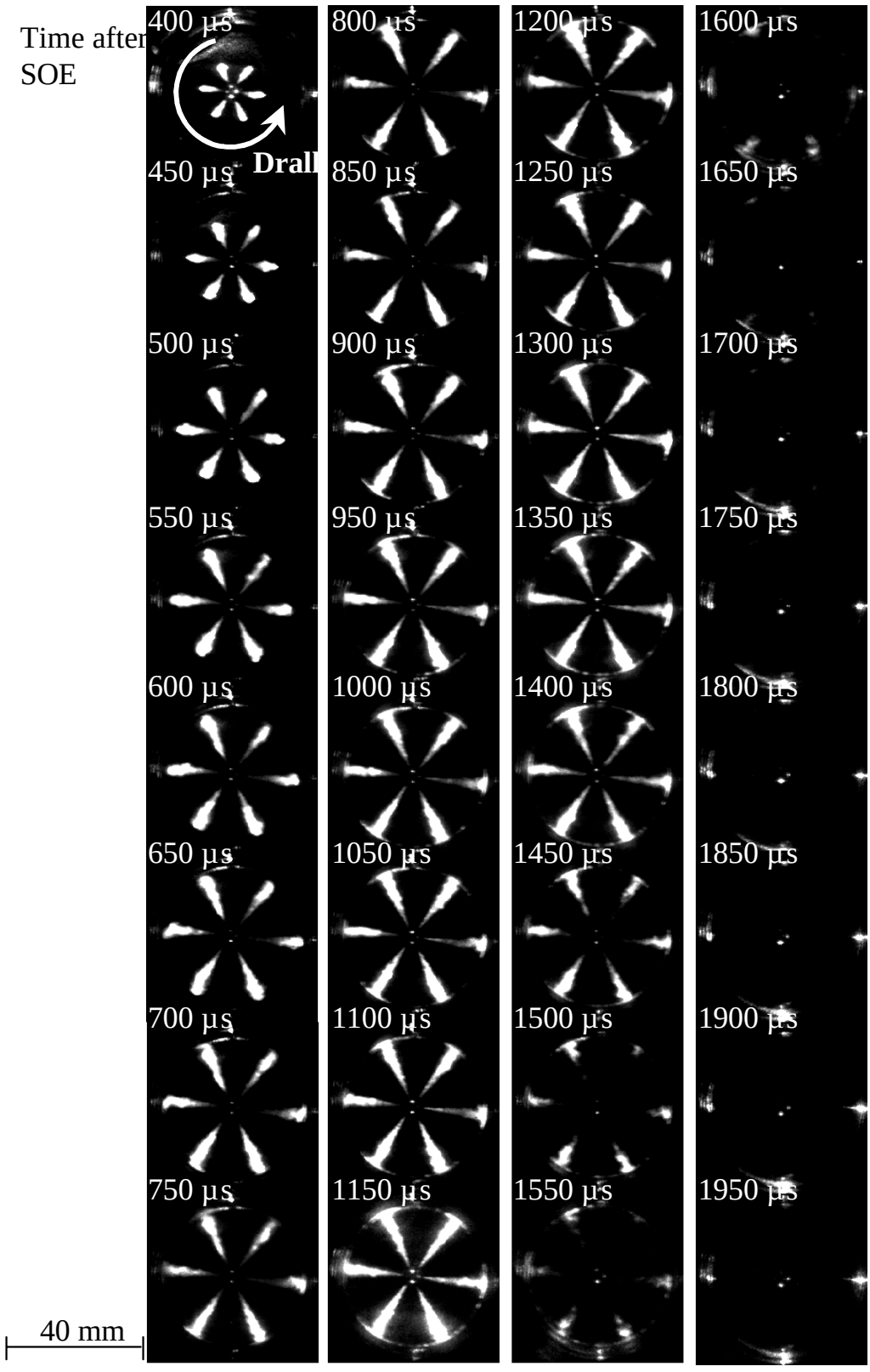

Figure 7 Temporal evolution of the spray into the combustion chamber using an Ω-shaped piston crown. The sequence is constructed from four individual cycles. Times inserted to each image is relative to the trigger initiating injector operation. Notice that these images are distorted by the Ω-shaped bowl. Before data analysis these images have been corrected for distortion.

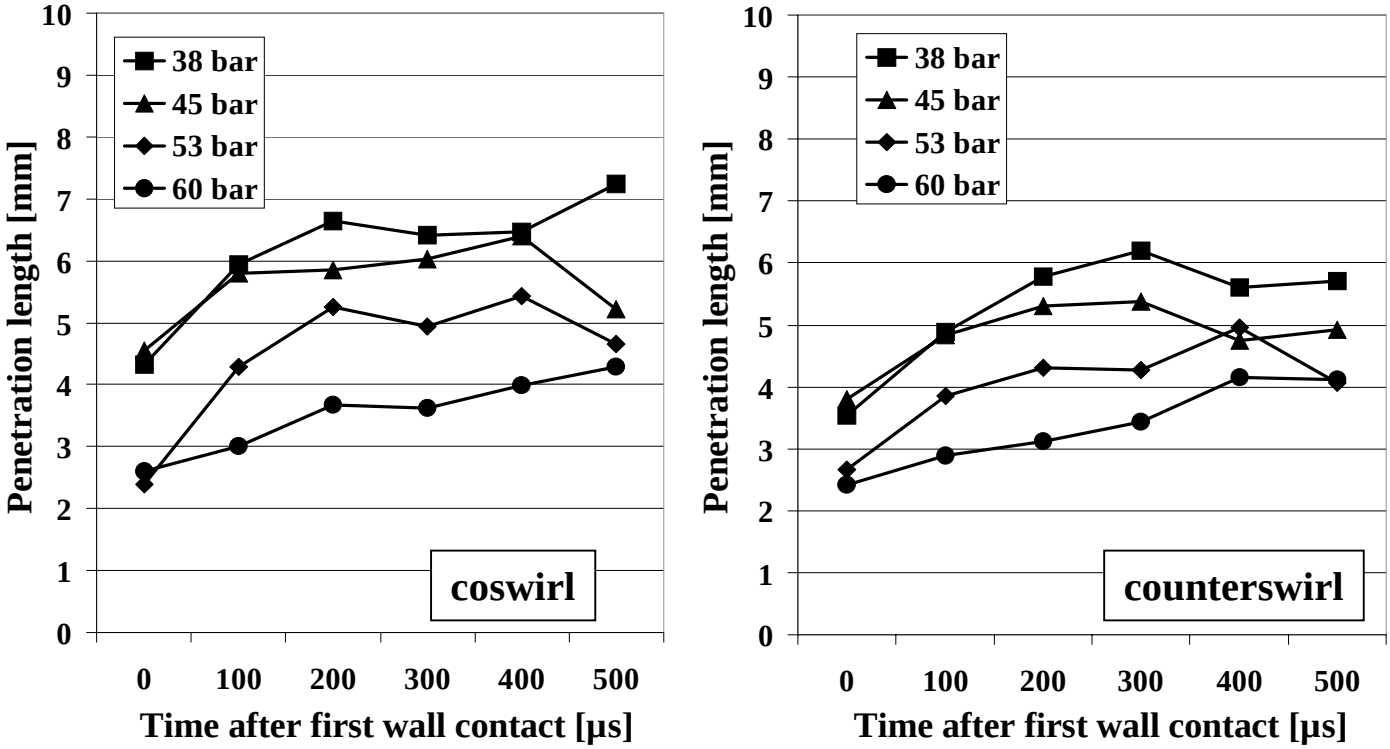

Figure 8 Spray penetration in tangential direction perpendicular to the initial direction of the spray expansion after impingement on the Ω-shaped piston wall. (a) penetration in clock-wise direction, (b) penetration in anti-clock wise direction. Penetration depths are relative to the location of initial spray impact on the wall. Pressure in the intake duct has been varied to change the cylinder pressure at TDC from 38, 45, 53 to 60 bar corresponding to intake duct pressures of 1000, 1200, 1400, and 1600 mbar, respectively.

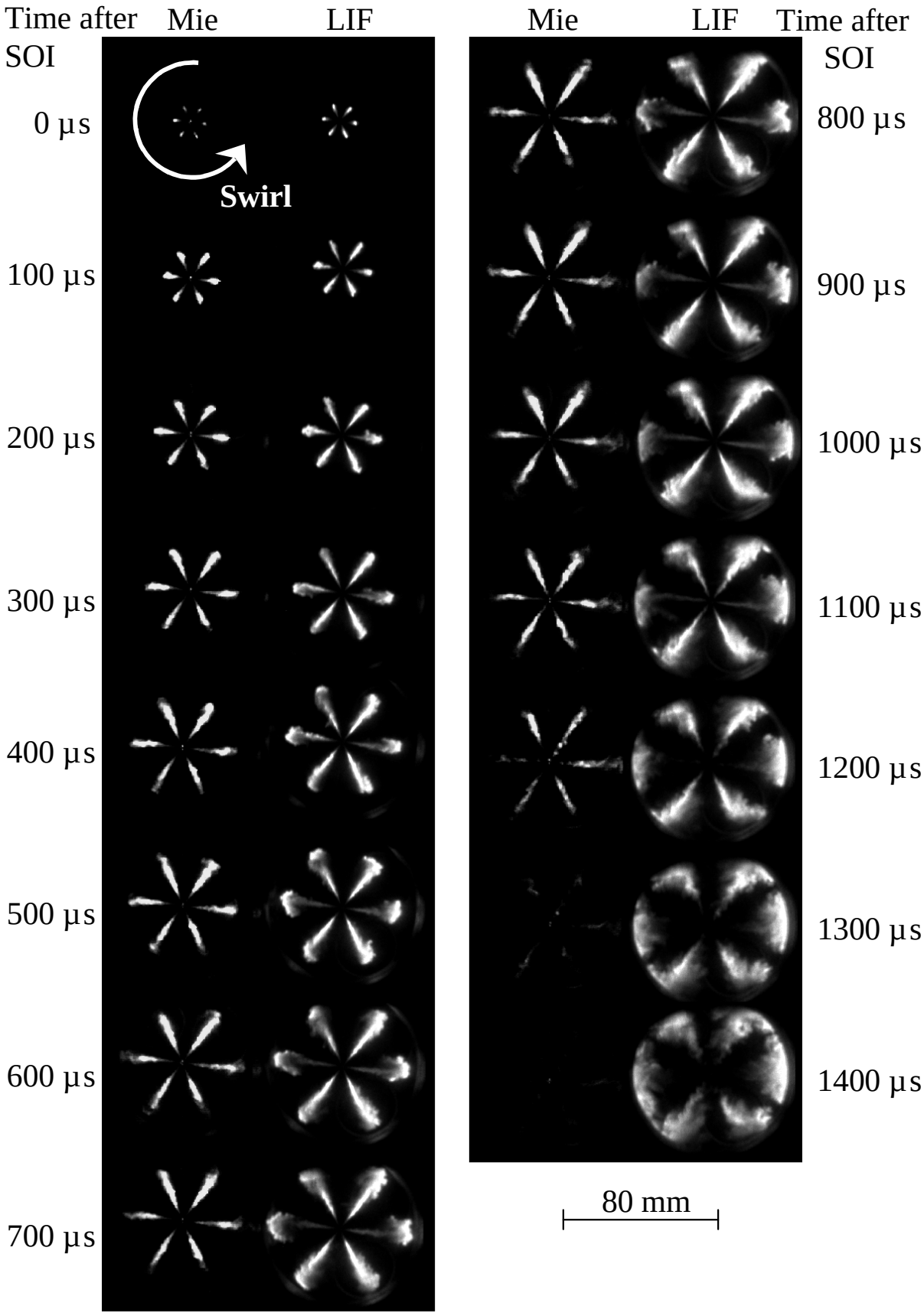

Figure 9 Temporal evolution of the spray using an injection pressure of 800 bar as observed by combined Mie/LIF diagnostics. Times are relative to the first observation of LIF signals. Conditions for the intake duct temperature and pressure are 25°C and 1600 mbar.

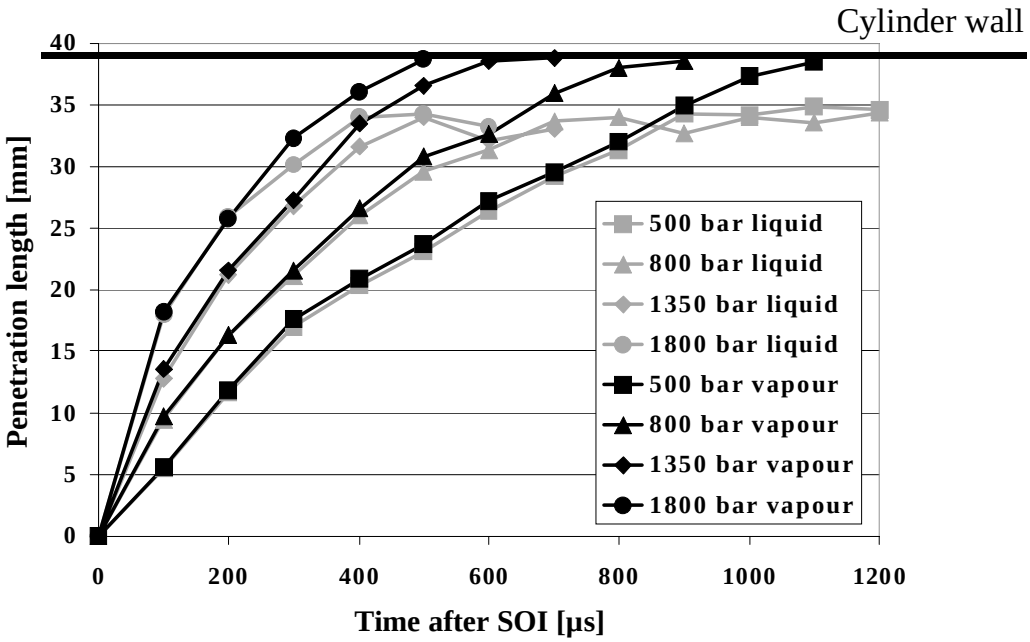

Figure 10 Temporal evolution of the spray patterns observed by fuel LIF (black symbols) and by Mie scattering (grey symbols) for different injection pressures. The fuel LIF represents both the liquid and the gaseous phase of the fuel while the Mie scattering visualises the liquid phase only. Notice, that due to the limited dynamic range of the detector used for the Mie technique the smallest droplet diameter is approximately 2 µm.

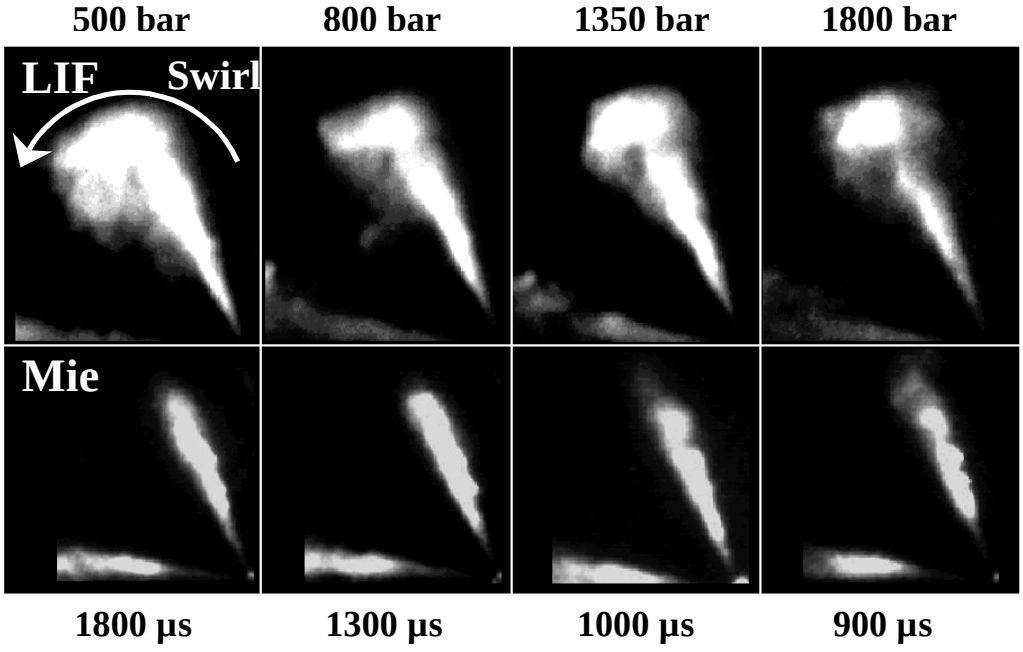

Figure 11 Single spray structures simultaneously observed by LIF and Mie scattering. Injection pressure has been varied from 500 to 1800 bar. For comparison corresponding process times have been selected as stated in the figure.

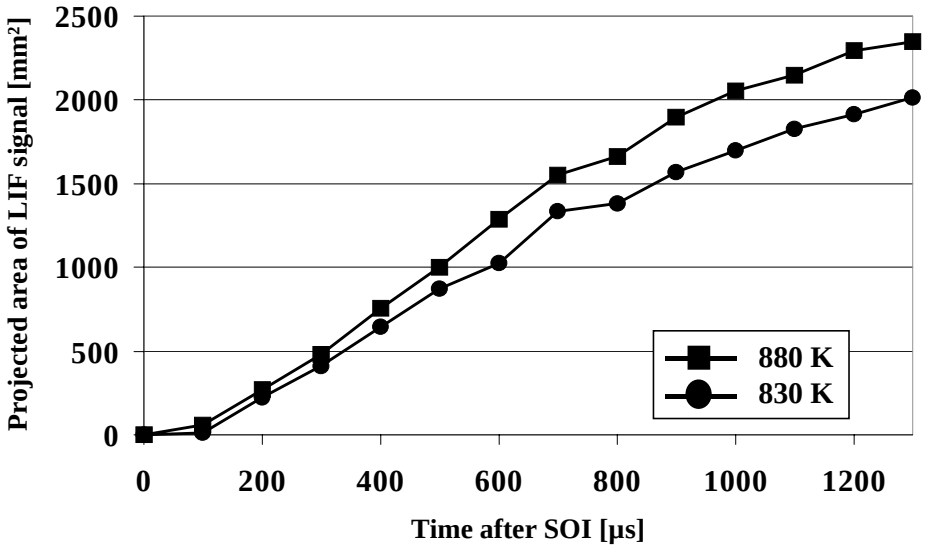

Figure 12 Area of the fuel LIF signal as function of process time. The figure visualises fuel evaporation for two different cylinder temperatures at TDC.

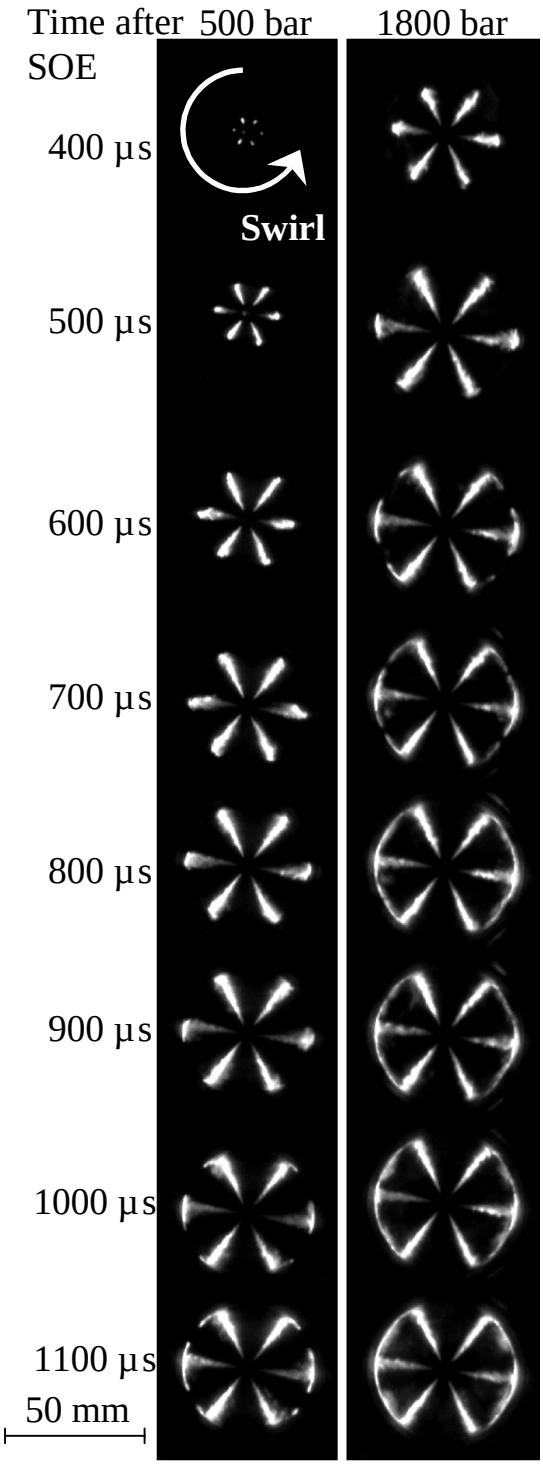

Figure 13 LIF sequences of liquid and gaseous fuel for different injection pressures. Intake duct conditions are 1600 mbar and 25°C. Times are relative to the trigger releasing the injection. Data shown are not corrected for optical distortion.

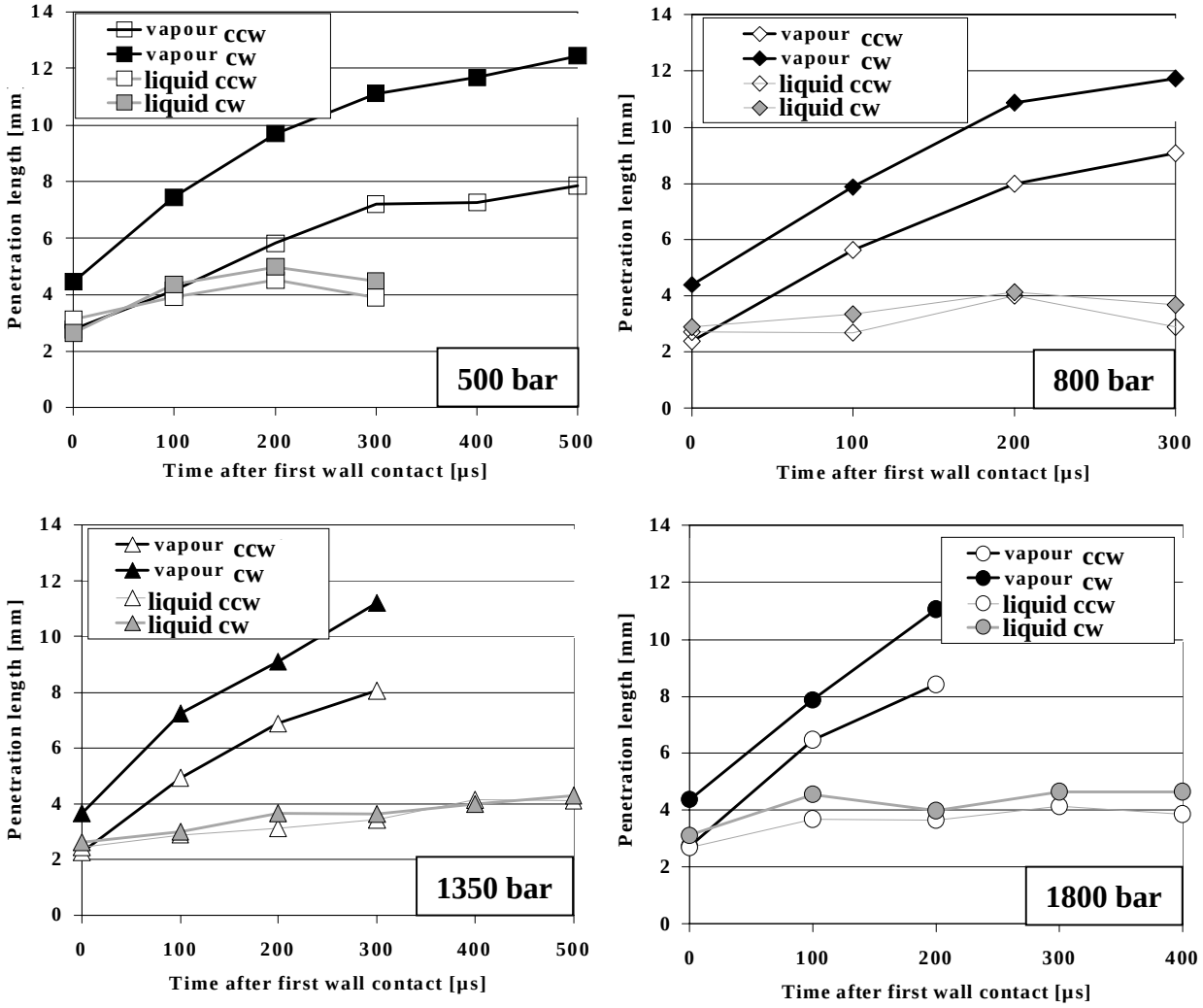

Figure 14 Comparison of penetration depth of liquid and gaseous fuel in clock- and anti-clock wise direction. Notice, that the swirl direction is anti-clock wise. Each plot presents data for different injection pressure as indicated by the insertion. Process times are relative to first impingement on the wall.

---

i Senda, J., Tanabe, Y., Fujimoto, H., Fukami, Y. „Visualization of evaporative Diesel spray impinging upon wall suface by exciplex fluorescence method" SAE Paper Series 920578 (1992).

ii Fujimoto, H., Kobayashi, M., Senda, J., Tanabe, Y. „Visualization and quantitative analysis of fuel vapor concentration in Diesel spray" JSAE Review 15, pp. 149 – 156 (1994).

iii Senda, J., Fujimoto, H., Kanda, T., Kobayashi, M. „Quantitative Analysis of fuel vapor concentration in Diesel spray by exciplex fluorescence method" SAE Paper Series 970796 (997).

iv Bardsley, M. E. A., Bracco, F. V., Felton, P. G. „2-D visualization of liquid and vapor fuel in an I.C. engine" SAE Paper Series 880521 (1988).

v W. Ipp, V. Wagner, H. Krämer, M. Wensing, A. Leipertz, S. Arndt und A.K. Jain, "Spray formation of high pressure swirl gasoline injectors investigated by two-dimensional Mie and LIEF techniques", SAE-Paper 1999 01 0498 (1999)

vi J. D. Naber, D. L. Siebers: Effects of Gas Density and Vaporisation on Penetration and Dispersion of Diesel Sprays, SAE Technical Paper No. 960034

vii D.A. Greenhalgh, J. B. Kelman, A.R. Masri, M.C. Jermy, G. Sherwood, Martin Berckmüller, Pulsed Laser Imaging in practical combustion systems from 2D to 4D, Proc. SPIE Vol. 4076 pp. 55-65 (2000)

viii A. Arnold, F. Dinkelacker, T. Heitzmann, P. Monkhouse, M. Schäfer, V. Sick, J. Wolfrum, W. Hentschel, K.P. Schindler: "DI Diesel Engine Combustion visualized by combined Laser Techniques", Twenty–Fourth Symposium (International) on Combustion/The Combustion Institute 1992/pp. 1605–1612

ix Löfström, C., Engström, J., Richter, M., Kaminski, C., Johansson, P., Nyholm, K., Hult, J., Nygren, J., Aldén, M. „Feasibility studies and application of laser /optical diagnostics for characterisation of a practical low-emission gas turbine combustor"ASME 2000-GT-124.

x Styron, J. P., Kelly-Zion, P. L., Peters, J. E., White, R. A., Lucgt, R. P. „Multicomponent liquid and vapor fuel distribution measurements in the cylinder of a port-injected spark ignition engine“ SAE Paper Series 2000-01-0243 (2000).
xi Melton, L. A., "Exciplex based vapor/liquid visualization systems appropriate for automotive gasolines" Applied Spectroscopy 47, Number 6, Society of Applied Spectroscopy (1993).
xii Bodwitch, F, W. “A new tool for combustion research – a quartz piston engine“ SAE transactions, Vol. 69, pp. 17 – 23 (1961).
xiii Uhl, M.: Simultane laseroptische Detektion der flüssigen und dampfförmigen Phase bei der Diesel-Direkteinspritzung, Thesis submitted at the Institut für Technische Verbrennung, University of Stuttgart (unpublished).
xiv D. L. Siebers: Scaling Liquid-Phase Fuel Penetration in Diesel Sprays Based on Mixing-Limited Vaporisation, SAE Technical Paper No. 1999-01-0528
xv Uhl, M.: Simultane laseroptische Detektion der flüssigen und dampfförmigen Phase bei der Diesel-Direkteinspritzung, Thesis submitted at the Institut für Technische Verbrennung, University of Stuttgart (unpublished).
xvi Mohammadi, A., Miwa, K., Kidogucji, Y „High time-space resolution analysis of droplets behaviour and gas entrainment into Diesel sprays impinging on a wall“ ILASS Europe, Darmstadt September 11.-13. 2000.
xvii Katsura, N., Saito, M, Senda, J, Fujimoto, H. „Characteristics of a Diesel spray impinging on a flat wall“ SAE Paper series 890264 (1989).
xviii Ishikawa, N., Zhang, L. „Characteristics of air-entrainment in a Diesel spray“ SAE Paper Series 1999-01-0522 (1999).
xix Meingast, U., Reichelt, L., Renz, U., Müller, D., Heine, B. „Nozzle exit velocity measurements at multi orifice CR-nozzles“ ILASS Europe, Darmstadt, 11.-13. September, 2000.
xx Schugger, C., Meingast, U., Renz, U. „Time resolved velocity measurements in the primary breakup zone of a high pressure Diesel injection nozzle“ ILASS Europe, Darmstadt, 11.-13. September, 2000.